

Lawrence Berkeley National Laboratory

Lawrence Berkeley National Laboratory

Title

Sensitivity study of reliable, high-throughput resolution metrics for photoresists

Permalink

<https://escholarship.org/uc/item/3z20s8k8>

Authors

Anderson, Christopher N.
Naulleau, Patrick P.

Publication Date

2008-06-24

Sensitivity study of reliable, high-throughput resolution metrics for photoresists

Christopher N. Anderson,^{1,*} and Patrick P. Naulleau,²

¹*University of California, Berkeley, Applied Science & Technology Group,
Berkeley, CA 94720, USA*

²*Center for X-ray Optics, Lawrence Berkeley National Laboratory,
1 Cyclotron Road, Berkeley, CA 94720, USA*

**Corresponding author: cnanderson@berkeley.edu*

The resolution of chemically amplified resists is becoming an increasing concern, especially for lithography in the extreme ultraviolet (EUV) regime. Large-scale screening and performance-based down-selection is currently underway to identify resist platforms that can support shrinking feature sizes. Resist screening efforts, however, are hampered by the absence of reliable resolution metrics that can objectively quantify resist resolution in a high-throughput fashion. Here we examine two high-throughput metrics for resist resolution determination. After summarizing their details and justifying their utility, we characterize the sensitivity of both metrics to two of the main experimental uncertainties associated with lithographic exposure tools, namely: limited focus control and limited knowledge of optical aberrations. For an implementation at EUV wavelengths, we report aberration and focus limited error bars in extracted resolution of ≈ 1.25 nm RMS for both metrics making them attractive candidates for future screening and down-selection efforts. © 2007 Optical Society of America

OCIS codes: 100.2000 (Digital Image Processing), 110.3960 (Microlithography), 100.3190 (Reverse Problems), 070.2580 (Fourier Optics), 070.2590 (Fourier Transforms).

1. Introduction

As lithography pushes to smaller and smaller feature sizes, the fidelity of chemically amplified resists becomes an increasing concern. This is especially true in the extreme ultraviolet

aerial image to a latent deprotection profile through a simple convolution process. Due to the simplicity of this model, extracting the effective resist blur from printing data is a relatively straightforward process.

Models based on the linear systems PSF approach are convenient because they provide an intuitive link to the resist resolution limit. As with many resist models, their success relies on the ability to accurately predict the aerial image incident at the wafer surface. In practice, limited knowledge of the experimental conditions in any given exposure hampers our ability to accurately model the aerial image. With exposure tools constantly pushing the limits of their imaging optics, the sensitivity of the aerial image to small changes in aberrations and focus is a possible concern for the success of PSF-based metrics. As an illustrating example we consider these effects for an implementation at EUV wavelengths. The parameters we describe correspond to the those found at the SEMATECH Berkeley microfield exposure tool (MET) printing facility [11].

The focus steps in a typical focus-exposure-matrix (FEM) at the Berkeley facility are on the order of 50-nm. Assuming that nominal focus is somewhere in the FEM, the random variable associated with aerial image defocus of the best-focus row in the FEM is uniform on the interval $[-25, 25]$ nm with a standard deviation of ≈ 14 -nm. For high-resolution exposure tools such as the 0.3 numerical aperture (NA) SEMATECH Berkeley MET, this magnitude of defocus may be enough to noticeably reduce aerial image contrast at high spatial frequencies.

Regarding aberrations, the RMS error in interferometrically measured aberrations of the SEMATECH Berkeley MET optic is 0.1545 nm [13], corresponding to a $\approx 10\% - 20\%$ error-bar in reported Zernike coefficients used in aerial image modeling software. With error bars of that magnitude one would expect an upper limit on the ability to accurately model the aerial image as printed feature sizes shrink towards the diffraction limit of the imaging optic. With exposure condition knowledge always limited to some extent, it is of interest to investigate the impact this has on the ability of PSF-based resolution metrics to extract credible resolution numbers.

3. Two reliable, high-throughput resolution metrics

The utility of a resolution metric is arguably best described by its ability to produce robust, credible results that agree with observed resolution limits. In practice, metric utility can also be characterized by an efficiency measure, or by the amount of exposure tool use-hours, SEM images, and modeling support that is required for reliable resolution extraction. In efforts to find high-throughput resolution metrics suitable for large-scale screening and resist down-selection, we study metrics that require < 10 SEM images and are relatively low overhead in terms of modeling support needed for blur extraction.

3c show SEM images of the corner of a 700-nm elbow at dose-to-size [14] taken at identical magnifications in EUV2D and MET1K resists. It is well known that MET1K supports higher resolutions than EUV2D [6]; the larger corner-rounding present in the EUV2D platform is consistent with the predictions of the PSF model. We extract resolution with this metric by comparing the amount of experimental corner rounding in a large, isolated feature to the amount of corner rounding in the equivalent modeling data with varying degrees of resist blur.

To quantify the amount of rounding in a given corner, we have developed and tested three different methods and down-selected to the one with the least sensitivity to unavoidably noisy experimental data. We settled on a metric that uses the removed area to indirectly compute an effective corner radius. As shown in Figure 4, we use in-house software to take radial line-outs of an experimental (or modeled) dose-to-size image to extract a radius vs. angle profile of the experimental (modeled) corner edge. By extrapolating the flat parts of the elbow out to the ideal (non-rounded) corner location we are able to generate a radius vs. angle profile for the ideal corner edge and compute the area that has been removed in converting the aerial image to a printed resist image.

With our two target resolution metrics summarized, we turn to determining the ability of each metric to extract meaningful and credible resolution numbers in the presence of unavoidable experimental uncertainties associated with exposure tools.

4. PSF-based resolution metrics: sensitivity to focus and aberrations

All PSF-based resolution metrics require aerial image modeling for resolution extraction. In this report all aerial images are generated using in-house software that supports arbitrarily defined optical aberrations, tunable defocus and customizable pupil fills [17]. For our specific implementation at EUV wavelengths, the base modeling parameters are set to match the experimental conditions of the SEMATECH Berkeley MET so that modeling data can be directly compared to experimental data obtained at the Berkeley facility. This includes a $5\times$ reduction imaging configuration, $\sigma = 0.35 - 0.55$ annular pupil fill and optical aberrations set to match the aberrations measured during the initial interferometric SEMATECH Berkeley MET tool alignment [13].

4.A. Corner metric

For the implementation at EUV wavelengths, our object of choice is a dark-field 700-nm elbow (the elbow is bright). To model the 700-nm elbow, we assume a thin (binary), idealized mask as an approximation to the realistic e-beam-written, multilayer-coated EUV mask. We believe these approximations to be reasonable owing to the fact that in terms of corner fidelity, the feature size of interest is very large relative to the 13.5 nm wavelength being

4.B. Contact metric

Focus. For the contact metric, our modeled object is a 300×300 nm patch of 50-nm, 150-nm pitch, dark-field contacts (the contacts are bright), which through sampling effects is equivalent to modeling an infinite 2D array of contacts. We again assume an ideal thin (binarized) mask. To generate blurred aerial images through focus, we follow a procedure identical to that outlined in the corner metric section. For contacts, we define the nominal plane of best focus as the plane with the highest average (un-blurred) aerial image contrast when the aberrations are set to match our base standard.

For each modeled focus-blur combination, we use in-house software to measure the contact diameter (CD) through dose (or equivalently, threshold) and generate a CD vs. relative dose curve. Relative dose is obtained by normalizing absolute dose (threshold) to dose-to-size; each focus-blur combination has a unique dose where this occurs. Figure 7 shows the family of these curves for 5 focus steps spanning $[-50, 50]$ nm defocus and for blurs ranging from 0 to 35 nm in 5 nm steps. The series of focus curves within a given blur level are plotted with the same graylevel and there are different graylevels for each blur level. Note the curves in the 0 nm and 5 nm blur levels overlap heavily. We do not process the larger blurs (40, 50, 60 nm) for the contact metric as they severely reduce the contrast in the deprotection image.

To work out the focus-limited error bars we use a least-squares approach. We start by generating CD vs. relative dose curves at nominal focus and base aberrations for blurs spanning 27.5-32.5 nm in 0.25 nm steps; we call these the nominal curves. Then for each defocused trial curve in the 30-nm blur level we find the nominal blur curve that most closely resembles the trial curve in terms of least-squared-error (LSE). By cataloging the range of modeled nominal blurs spanned by the series of defocused trial curves we report focus-limited error bars of 1.70 nm peak-to-valley and 0.83 nm RMS.

Aberrations. Aerial images are generated following the procedure outlined in the corner rounding aberrations section. For each of the 10 images at a given noise level (10%, 20%, and 30%) we generate CD vs. relative dose curves for blurs ranging from 0 to 35 nm in 5 nm steps and plot them so that the series of 10 random aberration curves within a given blur level are plotted with the same graylevel, different graylevels for each blur level. Figure 8 shows the families of curves for RMS aberration noise levels of 0%, 10%, 20%, and 30%. To work out the aberration-limited error bars for a given noise level, we use the same least-squares approach as in the focus study except the target curves we fit to have changed as a result of aberrations, not defocus. Table 2 summarizes the aberration-limited error bars for the contact metric.

blurs. For blurs < 5 nm, the error bars become a sizable portion ($> 50\%$) of the blur value, rendering both metrics useless in this regime.

We note, however that it is reasonable to assume a minimal fidelity loss in converting the aerial image to a deprotection profile when the resist blur is much smaller than the PSF-blur of the imaging optic. The resolution of the SEMATECH Berkeley MET optic is ≈ 22 nm [11]. That said, we expect to see very little difference in printing for resists with blurs < 5 -10 nm for our EUV implementation. Of course, as the resolution of the lithography tool improves, we would expect the utility of both resolution metrics to extend into the sub-5-nm blur regime. For example, we would expect to have no problem measuring a 5 nm resist blur with an 8 nm e-beam tool provided the 8 nm tool aberrations are characterized well enough to allow the aberration-limited error bars to support this measurement.

The sources of error described here can be categorized into a group of errors that limit the ability to accurately model the aerial image at the wafer surface in a given exposure. As we have seen, these model-limiting error sources put constraints on the credibility of resolution numbers extracted with the corner and contact metrics. In addition to these error sources, there are other errors that affect the credibility of extracted resolution numbers. One example to study is how SEM focus affects the measured CD and corner rounding numbers. Another example to look at is how tool dose errors affect the slopes of the measured CD vs. dose curves (note this only applies to the contact metric). We are also interested in studying how LER impacts our analysis software in terms of consistently delivering the same CD and rounding numbers for different copies of the same coded feature. Another useful thing to study would be the shot-to-shot variations in extracted CD and corner rounding for a full FEM of identically prepared features. In a way, this study could essentially lump the effects of SEM focus, tool focus and LER into a full process error bar.

6. Summary

In this paper we have studied two high-throughput PSF-based photoresist resolution metrics, justified their utility and characterized their sensitivity to two uncertainties associated with exposure tools, namely: limited knowledge of focus and limited knowledge of optical aberrations. In our specific implementation at EUV wavelengths with exposure conditions matching those at the SEMATECH Berkeley MET printing facility, modeling suggests that PSF-based resolution metrics have focus and aberration limited error bars in extracted resolution of ≈ 3 nm peak-to-valley and 1.25 nm RMS. As the PSF-based metrics considered here require minimal exposure data and relatively low overhead in terms of modeling support and SEM images, they are attractive platforms for large-scale resist screening and down-selection efforts.

The authors are greatly indebted to Paul Denham, Ken Goldberg, Brian Hoef, Gideon

12. A.J.E.M. Janseen, "Extended Nijboer-Zernike approach for the computation of optical point-spread-functions," JOSA A Vol. 19, p. 849 (2002).
13. K. Goldberg, et al. "At-Wavelength Alignment and Testing of the 0.3 NA MET Optic," J. Vac. Sci. and Technol. B 22, 2956-2961 (2004).
14. As an external control, all experimental and modeling corner data is taken at and around the dose where the coded 100-nm features print at 100-nm.
15. G. Gallatin, "Resist Blur and Line Edge Roughness," Proc. SPIE 5753, 38-52 (2005).
16. F. Houle, W. Hinsberg, M. Morrison, M. Sanchez, G. Wallraff, C. Larson, and J. Hoffnagle, "Determination of coupled acid catalysis-diffusion processes in a positive-tone chemically amplified photoresist," J. Vac. Sci. and Technol. B 18, 1874-1885 (2000).
17. Note that commercial modeling packages such as PROLITH and SOLID E could also be used.
18. P. Naulleau, C. Anderson, K. Dean, P. Denham, K. Goldberg, B. Hoef, B. La Fontaine, and T. Wallow "Recent results from the Berkeley 0.3-NA EUV microfield exposure tool," Proc. of SPIE 6517 (2007)

22	Aberration-limited error-bars for the corner rounding metric ^a
23	Aberration-limited error-bars for the contact metric ^a

List of Tables



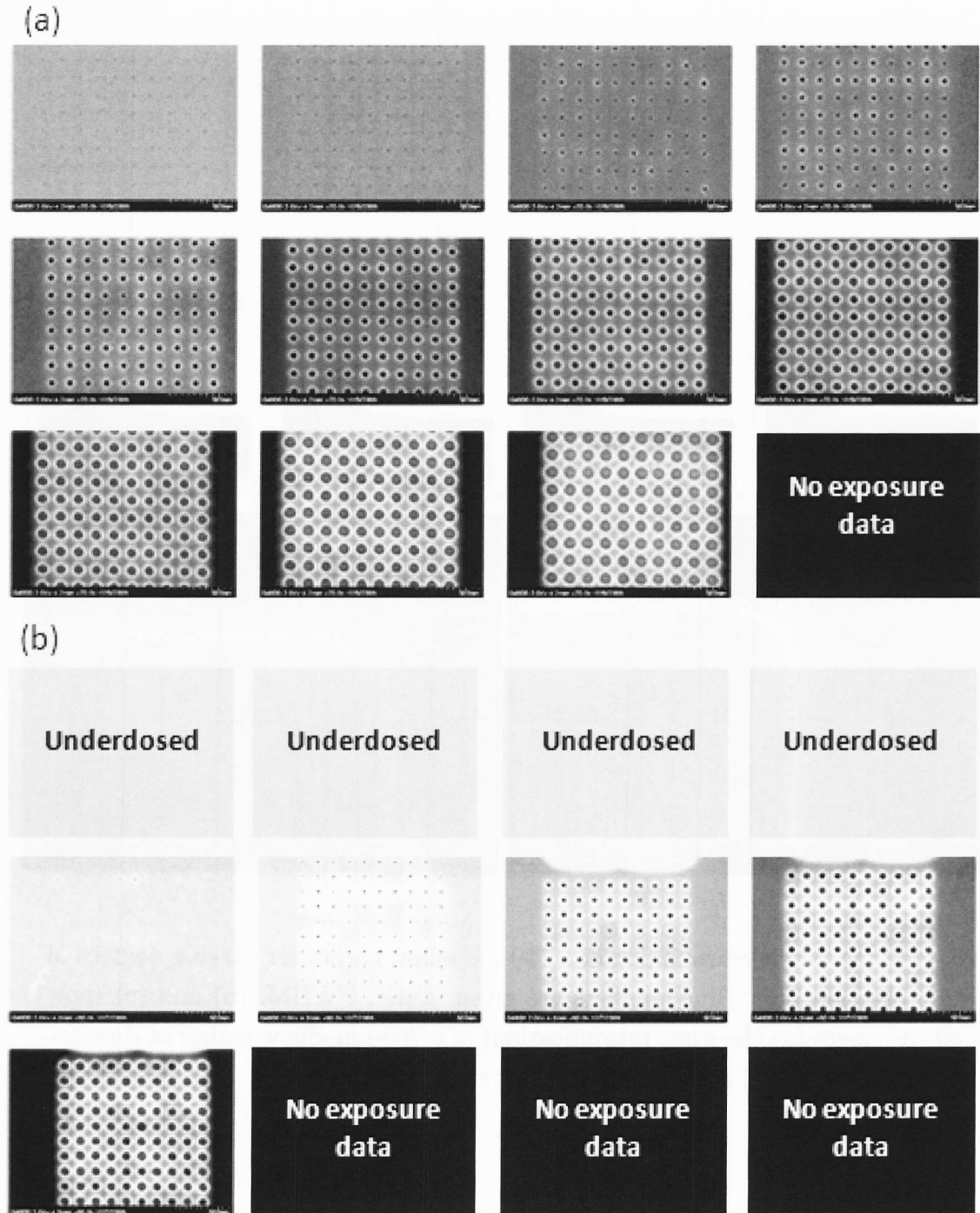


Fig. 2. Through-dose 50-nm contact printing in MET1K (a) and EUV2D (b) resists with 15% relative dose steps between exposures.

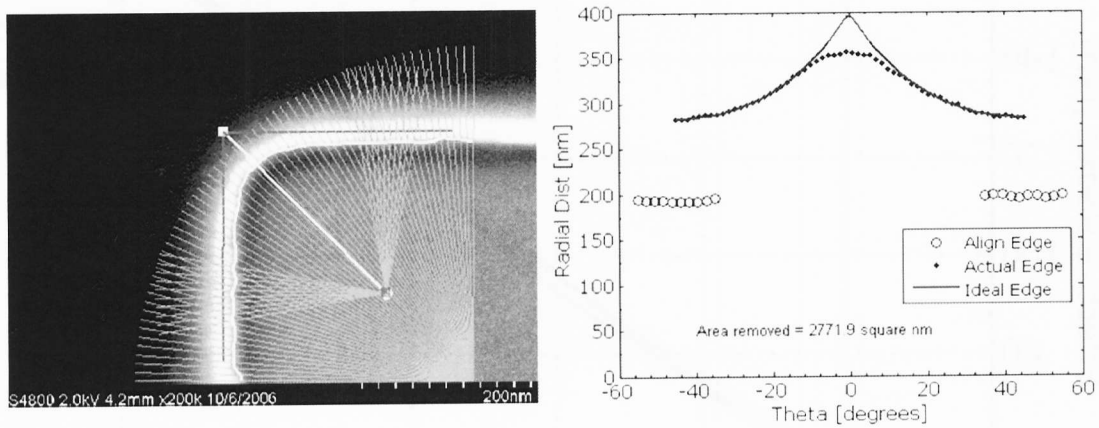


Fig. 4. Screenshot of in-house software used to extract corner rounding from an experimental SEM image. The plot to the right shows the radial line-outs for the ideal (non-rounded) and actual (rounded) corner edges.

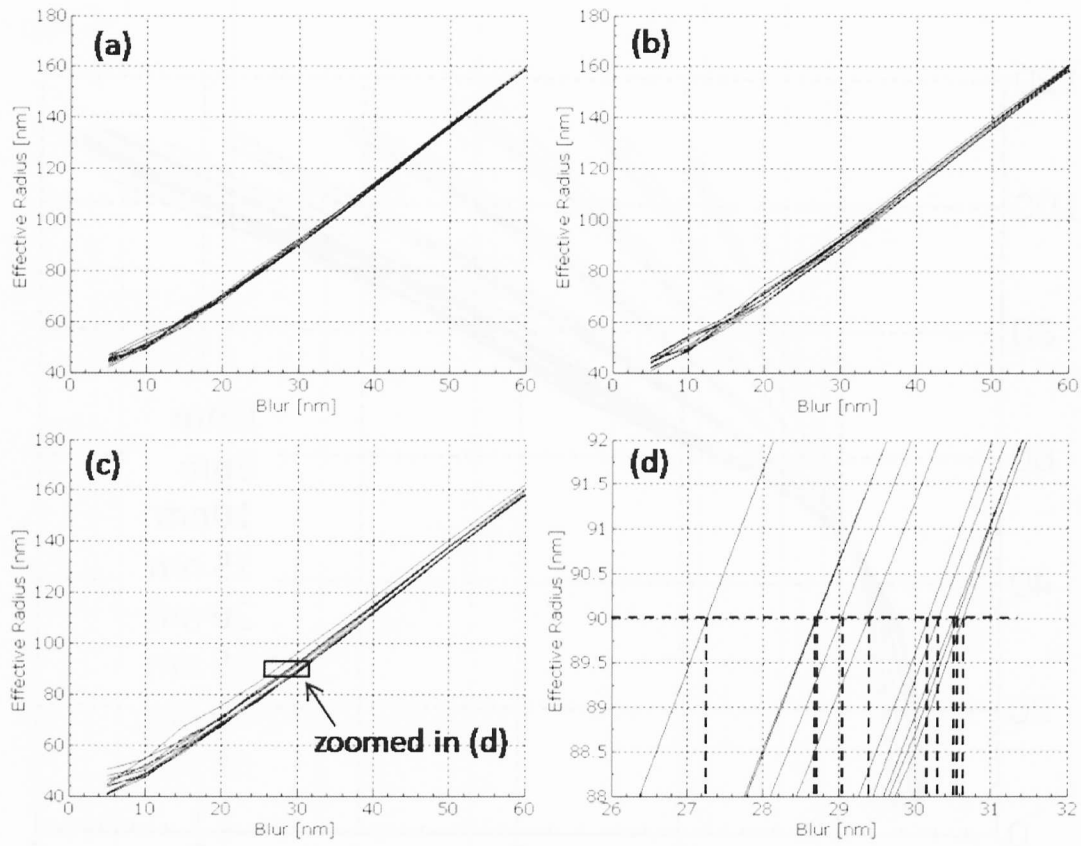


Fig. 6. Corner rounding vs. blur curves for the families of random aberration maps in the 10% (a), 20% (b), and 30% (c) RMS noise levels. (d) Zoomed 30% noise plot centered around the radius of 90 nm. Solid lines indicate modeled radius vs. blur data for the 10 aberration maps in the 30% noise level. The intersections of the horizontal dashed line at radius = 90 nm with the 10 modeled curves are traced down with vertical dashed lines to show the range of blurs that might produce a rounding of ≈ 90 nm assuming a 30% RMS uncertainty in optical aberrations.

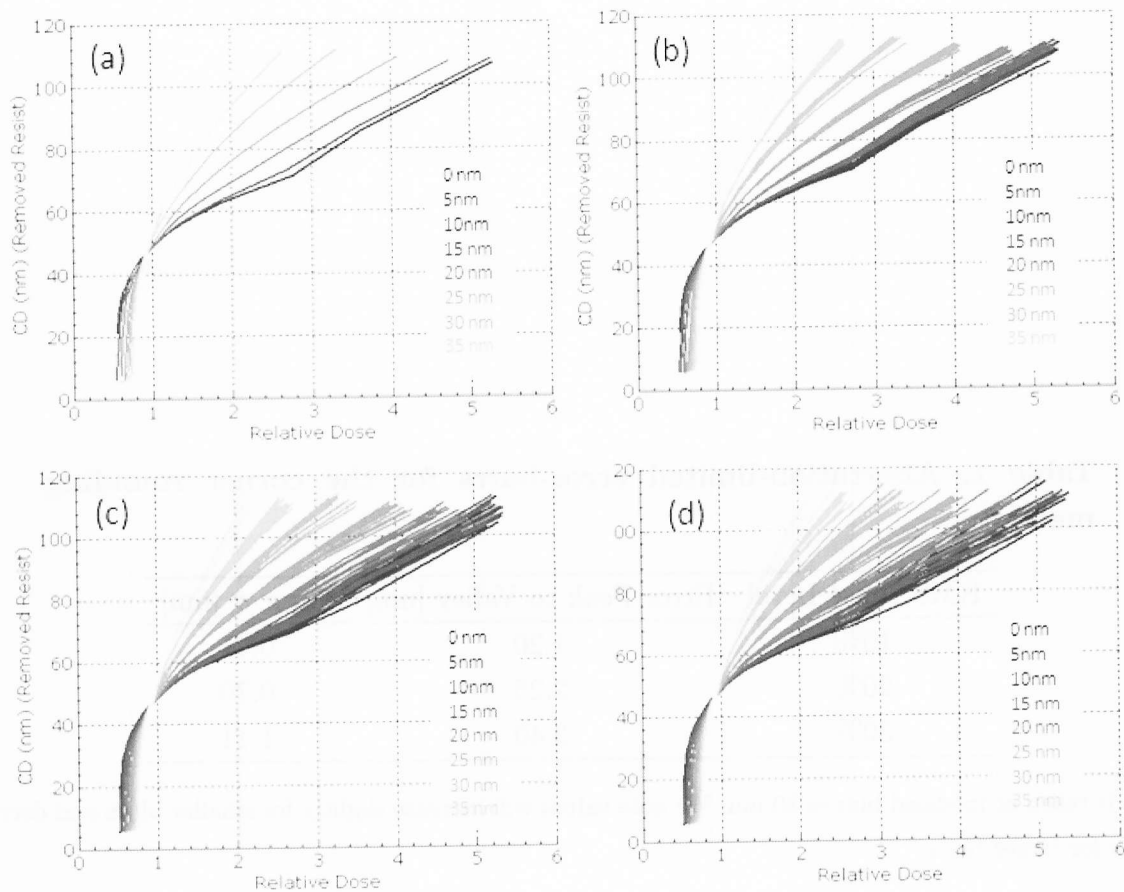


Fig. 8. (a) CD vs. relative dose curves for modeled deprotection blurs of 0-35 nm in 5 nm steps. Steeper slopes and lighter shades are larger blurs. (b), (c) and (d) show the same curves for the families of random aberration maps in the 10%, 20%, and 30% RMS noise levels, respectively. All random aberration maps within one blur are plotted with the same color. Note the heavy overlap of the 0 nm and 5 nm blur level curves.

Table 2. Aberration-limited error-barrs for the contact metric^a

RMS Noise Level	Error Peak to Valley [nm]	Error σ [nm]
10%	1.40	0.46
20%	2.85	0.91
30%	4.90	1.53

^aData is taken at modeled blur ≈ 30 nm. We note values will increase slightly for smaller blurs and decrease slightly for larger blurs.